Nanoscale

RSC Publishing

PAPER

View Article Online
View Journal | View Issue

How do the electron beam writing and metal deposition affect the properties of graphene during device fabrication?

Cite this: *Nanoscale*, 2013, **5**, 3352

Xiaonan Shen,[a] Haomin Wang[a] and Ting Yu*[abc]

Electron beam exposure and metallic contact formation are commonly used processes for fabrication of graphene-based devices. We report a detailed Raman study on the influence of medium energy electron irradiation and metal atoms on defectivity and doping on monolayer and bilayer graphene. It is found that the electron beam could induce disorder into graphene layers mainly by three ways: knocking-off carbon atoms, reaction with substrate and deposition of amorphous carbon. We observe that bilayer graphene exhibits higher stability under e-beam irradiation than monolayer graphene. Our study on the formation process of metallic contacts reveals that evaporation of Ti normally cannot induce any defects into graphene while deposition of Au can introduce a large amount of damage. This work could be valuable for further development of processes in the fabrication of graphene-based devices.

Received 3rd November 2012
Accepted 4th February 2013

DOI: 10.1039/c3nr33460k

www.rsc.org/nanoscale

Fabrication of graphene-based devices often requires the use of many different techniques and processes, like scanning electronic microscopy, electron beam lithography and physical vapor deposition.[1] These may introduce energetic bombardment on the graphene lattice. As graphene is as thin as a single atomic layer, the bombardment could cause a change of the lattice structure in graphene even at low dosages. This change may significantly alter the physical properties of graphene, like the carrier transport and thermal conductivity. Due to the practical importance, many researchers have carried out investigations on the influence of energetic irradiation on graphene properties.[2–9] Some investigations suggest that electron beam (e-beam) irradiation may transform graphene into small crystallites and then amorphous carbon.[3,4] Some interpretations emphasize that e-beam irradiation converted graphene into graphane through reversible hydrogenation or made graphene partially hydrogenated with adsorbates such as H_2O.[5,8] Some others believe that the electron-beam promotes reduction of the underlying SiO_2 and creates mobile oxygen, which could induce oxidation of the graphene layer.[6,7] There appears to be no broad consensus on a clear profile about the influence of e-beam irradiation. More importantly, graphene is covered with e-beam resist in actual lithography processing. It is not directly exposed to e-beam bombardment. Therefore, further investigations are necessary to understand the e-beam irradiation phenomena on graphene systems during device fabrication. Besides electron irradiation, metal atoms' bombardment can damage the graphene lattice more seriously than electrons in the contact formation of devices. This is mainly because of two major causes. Firstly, metal atoms are much more massive than electrons and they may carry larger momentum. Secondly, metal atoms are directly deposited onto the graphene surface in actual processing. Metals (like Ti, Au) are widely used as contacts for graphene devices. Previous studies have revealed that graphene is quite sensitive to metal irradiation, leading to electronic doping and scattering.[10,11] Although the effect of doping these metals on the electronic properties of graphene has been known, a detailed investigation of lattice variation after metal deposition is still lacking. In this paper, we discuss the electron and metal-atom bombardment effects on graphene in actual device fabrication processing, and use Raman spectroscopy to characterize these effects.

In this experiment, the Raman spectra were acquired by a WITEC CRM200 Raman system. The excitation source was a 532 nm laser (2.33 eV) with laser power below 0.1 mW in order to avoid any damage to the graphene. A 100× objective lens with a Numerical Aperture (NA) = 0.95 was used in the Raman measurements, and the spot size was about 500 nm in diameter. AFM images on different surfaces were recorded in tapping mode (VeecoNanoScope V AFM) using AppNano ACT-30 AFM tips of nominal radius of less than 10 nm. AFM images were not flattened or smoothed. Electron beam irradiation was carried out in an AURIGA FIB-SEM CrossBeam® Workstation system equipped with a nanopatterning system. The accelerating voltages and probing current were fixed at 20 keV and 20 pA. A Keithley 4200 semiconductor characterization system was used

[a]*Division of Physics and Applied Physics, School of Physical and Mathematical Sciences, Nanyang Technological University, 637371 Singapore, Singapore. E-mail: yuting@ntu.edu.sg*

[b]*Department of Physics, Faculty of Science, National University of Singapore, 117542 Singapore, Singapore*

[c]*Graphene Research Center, Faculty of Science, National University of Singapore, 117546 Singapore, Singapore*

to record the electrical properties of these devices. The resistance (R) *versus* gate voltage (V_g) curve was recorded with the drain–source bias at 0.1 V.

First, we adapted micro-Raman spectroscopy and atomic force microscopy (AFM) to study in detail the effect of the e-beam on pristine exfoliated graphene in order to understand how the disorder is introduced in the material through energetic electron irradiation. The graphene flakes were peeled-off from natural graphite using Scotch tape and transferred onto a silicon substrate capped with a 300 nm SiO_2 layer. The flakes are single-layer graphene (SLG) and typically 20–100 μm^2 in size. An optical microscope was used to locate the graphene sample[12] and Raman spectroscopy was used to identify the thickness of the graphene.[13] Fig. 1(a) shows an optical image of one SLG sample on SiO_2/Si substrate and its AFM height image and Raman spectrum are shown in Fig. 1(b) and (c), respectively. Four squares (indicated in Fig. 1(d)) of 3×3 μm^2 are irradiated with different electron dosages of 0.03, 0.3, 3 and 30 nC μm^{-2}, highlighted by red, blue, green and purple dashed line frames, respectively. After electron beam irradiation, the two square regions subjected to more severe irradiation (3 and 30 nC μm^{-2}) could be seen under the optical microscope. As shown in Fig. 1(e), the heights of these two squares appear to be about 1.8 nm and 3.4 nm, respectively, in the AFM topographic image. In order to further study the e-beam irradiation effects, Raman spectra were taken of the squares and are plotted in Fig. 1(f). The D peak, a well-known fingerprint of disorder in graphitic materials, appears after electron beam irradiation even at the lowest dosage of 0.03 nC μm^{-2}. The ratio of the intensity of D mode and G mode increases from 0.05, 0.86 to 2.75 with the increase of dosage from 0.03, 0.3 to 3 nC μm^{-2}. The enhancement of the D peak with the increase of electron dosage implies that more disorder was introduced into the graphene lattice. When the electron dosage was increased to as much as 30 nC μm^{-2}, G and D peaks become remarkably board and merge with each other partially, which are typical spectral features of highly disordered or amorphous carbon. The above results clearly show that there are additional layers of amorphous carbon on the graphene. The effect of the e-beam irradiation can be threefold. Firstly, an electron beam with high energy may damage the lattice structure in graphene. An earlier study in transmission electron microscopy (TEM) found that the high energy electron beam can knock away carbon atoms in graphene and induce defects like Stone–Wales defects and reconstructed vacancies.[14,15] Theoretical calculation suggests the energy barriers to overcome the Stone–Wales defects and vacancies in graphene are about 5 eV and 8 eV, respectively.[16] Some researchers believe that carbon atoms are knocked away or re-constructed in graphene.[3,4,7,17–19] Secondly, an amorphous carbon layer was deposited on the surface of the graphene, inducing disorder to

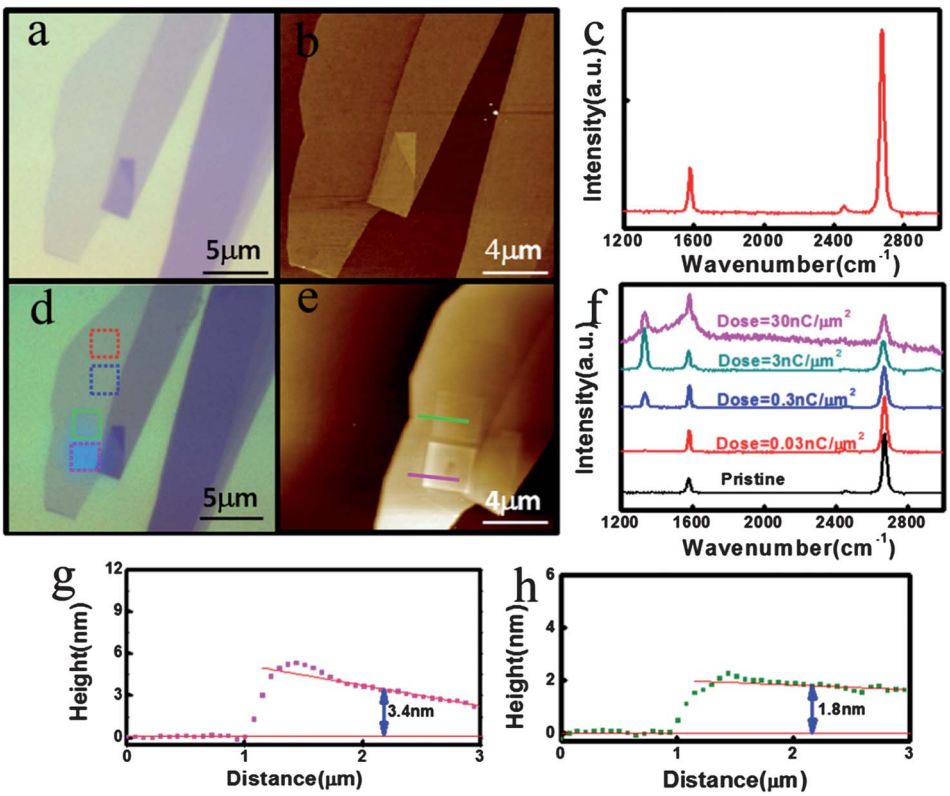

Fig. 1 Influence of electron beam irradiation on graphene: (a) optical and (b) AFM height image of a pristine graphene sample on SiO_2/Si substrate; (c) Raman spectrum of the monolayer region; (d) optical and (e) AFM height image of the same sample after e-beam irradiation. Four squares of 3×3 μm^2 are irradiated by an e-beam with dosages of 0.03, 0.3, 3, 30 nC μm^{-2}, respectively; (f) the corresponding Raman spectra from the squares with the corresponding color codes, together with the Raman spectrum of the pristine graphene. Raman intensities are normalized by the Si peak intensities; (g–h) height profiles for the two squares in (e), respectively.

the lattice system. This phenomenon did not attract enough attention in the previous studies on graphene. An electron beam always induces foreign atoms onto the graphene surface. Electron beam induced deposition in SEM has been studied for quite a long time. Organic contamination in the vacuum chamber would induce amorphous carbon films to be deposited on the substrate surface.[20,21] The amorphous carbon films could introduce defects in the graphene lattice similar to how adsorbates caused the partially hydrogenated graphene.[5,8,22,23] Thirdly, ions with kinetic energy (*e.g.* O^-, Si^-, Si^+, $Si^{2+}$and Si^{3+}) can be desorbed from the SiO_2 substrate when the electron energy is higher than 100 eV.[24] The energetic ions induced by the medium energy electrons could interact with graphene and induce defects in the graphene lattice.[25] All of the three reasons together may contribute to the appearance of defects in graphene sample. Continuous irradiation could introduce an additional amorphous carbon film on the graphene. When the electron beam dosage is as large as 30 nC μm^{-2}, the amorphous carbon thin film could be clearly seen under an optical microscope (Fig. 1(d)) and was reflected in the Raman spectrum (Fig. 1(f)).

Electron beam lithography (EBL) is widely used in device fabrication. In actual nanolithographic processing, graphene devices are not directly exposed to electron-beam irradiation. The electron-sensitive resist (polymethylmethacrylate, PMMA) covers the graphene surface. In this work, graphene samples were covered by 300 nm PPM (MMA) and 150 nm PMMA after the baking process. Electron beam lithography is adapted to create square windows (3×3 μm^2) on the graphene with an electron dosage of 0.004 nC μm^{-2}. After development, we can exam the effect of the e-beam exposure. Raman measurements were performed before and after the EBL process. Fig. 2(a) shows the optical image of pristine SLG and the same sample after EBL and developing. The corresponding Raman spectra are plotted in Fig. 2(b). It is very clear that there is a D peak in graphene after the EBL process. It indicates that the electron beam would induce defects in graphene even when covered with an e-beam resist. We did not observe any D peak outside the exposed windows. The results are different from the earlier report.[26] The same process was conducted on bilayer graphene (BLG) as comparison. The optical images and Raman spectra are shown in Fig. 2(c) and (d), respectively. The absence of a detectable D peak for the BLG after the EBL process indicates that BLG is much more robust to e-beam exposure compared to SLG. This may be due to their different energy barriers for defect formation. In this case, the direct deposition of amorphous carbon is fairly unlikely. Amorphous carbon can be lift-off after development of the resist. During the e-beam irradiation, the electrons travel through the resist and then reach the graphene surface.[27,28] Energetic electrons could interact with the graphene lattice. This interaction includes collisions between the electrons and carbon atoms, and ion desorption from the substrate. Defects may be induced by the interaction. Obviously, BLG has a higher energy barrier for defect formation than SLG. We noticed that the position of the G′ peak is red-shifted; this indicates that the electron irradiation causes an increasing of the electron concentration in graphene.[29] This allows the use of the G′ peak to discriminate between electron and hole doping.

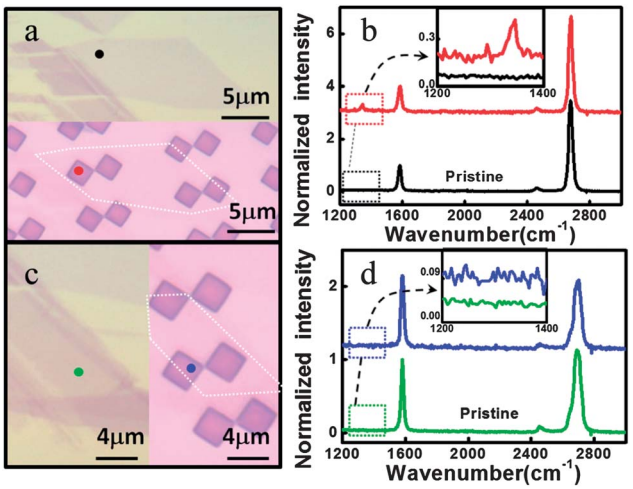

Fig. 2 Optical investigation of monolayer and bilayer graphene before/after the electron beam lithography process: (a) optical image of the bare monolayer (upper) and SLG coated with resist. The square parts were exposed to the e-beam and developed. The thickness of the e-beam resist is 300 nm and the e-beam is adapted with a dosage of 0.004 nC μm^{-2}. (b) Raman spectra of the SLG taken from the red and black spots in (a). The inset enlarges the range of D peak location for clarity. (c) Optical image of the pristine BLG and BLG coated with resist after development. The thickness of the resist and EBL dosage are the same as for SLG. (d) Raman spectra of BLG taken from the green and blue spots in (c), the inset enlarges the range of D peak location for clarity.

In the fabrication of graphene based devices, metals are always applied to graphene for the electrical contacts after nanolithographic processing. As gold (Au) electrodes with titanium (Ti) films as the adhesive layer are commonly employed on graphene based devices, we studied the effects of depositing these two metals on the lattice structure of graphene. Titanium and gold are deposited onto the surface of graphene by electron beam evaporation. The deposition of the metals atoms is calibrated by a crystal deposition monitor. Firstly, effects of coating a Ti thin film on both SLG and BLG are studied by Raman spectroscopy. 5 nm Ti thin film is deposited through electron beam evaporation onto the sample consisting of both SLG and BLG regions. Fig. 3(a) and (b) show the optical images of the sample before and after the deposition. The corresponding Raman spectra are plotted in Fig. 3(c) and (d), no D peaks were observed for both SLG and BLG with Ti coating. The results show that deposition of titanium is unlikely to introduce disorder to the graphene sample. The possible reason might be due to the very low kinetic energy of the Ti atom during the deposition.[30,31] In addition, we found that the deposition of Ti shifts the position of the G′ peak by about 10 cm^{-1} towards lower wavenumbers for single layer graphene. Electrical measurements on these graphene devices were carried out to analyze the influence of Ti deposition. Transport data are shown in Fig. 3(e). As shown in Fig. 3(e), the SLG device before Ti deposition is slightly p-type doped with the neutral point (NP) at 3 V. However, the NP shifts to −25.6 V after Ti deposition. Raman measurements were also performed on the graphene. It is found that the G′ peak red-shifts after Ti deposition and the D peak is absent. It indicates that the Ti atoms introduce n-doping

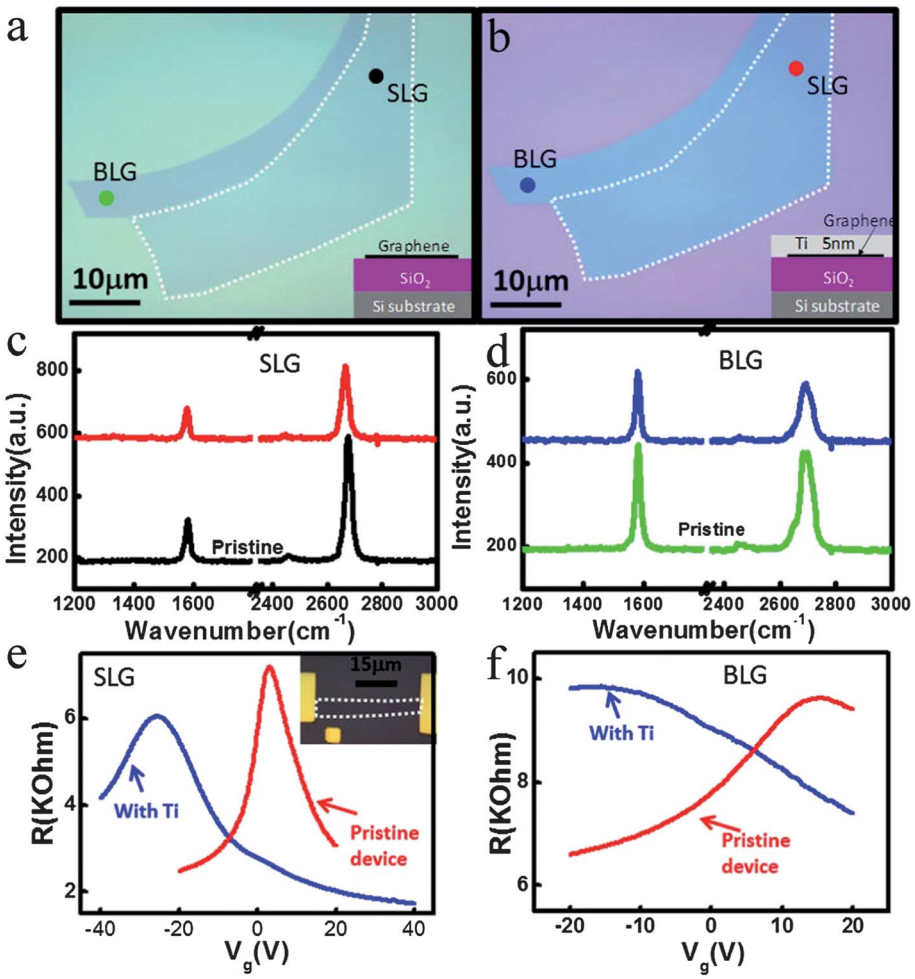

Fig. 3 Investigations on monolayer and bilayer graphene before/after exposing to Ti atoms' bombardment. (a) Optical image of pristine SLG and BLG. (b) Optical image of SLG and BLG after coating with 5 nm Ti. The insets of (a) and (b) show the schematic diagrams of the samples. (c) Raman spectra of SLG before and after depositing Ti. (d) Raman spectra of BLG before and after coating Ti. (e) Relationships of resistance and back gate voltage of SLG device before and after Ti deposition. (f) Relationships of resistance and back gate voltage of BLG device before and after Ti deposition.

in the graphene. The Raman results are consistent with that obtained from electrical measurement. And these findings are in good agreement with earlier literature.[11,29] In addition, electrical measurement on bilayer graphene was also carried out, and the results are shown in Fig. 3(f). The NP of BLG deposited with Ti shifts from 14.6 V (p-doping) to −16 V (n-doping), the results indicate that Ti also induces n-type doping in BLG. The n-type doping attributes to the charge transfer between Ti and graphene,[32–35] as the work function of monolayer graphene[36,37] ($\varphi_{graphene} \sim 4.5$ eV) is a little higher than that of Ti[38] ($\varphi_{Ti} \sim 4.3$ eV).

We deposited Au layers onto the surface of graphene *via* electron beam evaporation by using a shield mask (TEM grid with a bar width of 10 μm) to avoid too much damage.[39] An electrical contact of Ti/Au (5 nm/60 nm in thickness) is deposited onto the graphene. The spacing between mask and the substrate is about several micrometers, which is determined by the adhesive residue sitting in between the mask and substrate. Due to incomplete contact of the mask and substrate, the electrode metal typically invaded the electrode spacing below the shadow mask by tens of micrometers. We made use of this effect to study the influence of Au deposition on the graphene lattice. Raman spectroscopy was used to characterize the graphene samples after contact electrodes were deposited. As shown in Fig. 4(a), three different spots gradually farther away from the Au/Ti electrode were probed on monolayer graphene sheets. The corresponding Raman spectra are shown in Fig. 4(c), it is found that the D peak appears in the SLG close to the electrode and its intensity decreases for the SLG sheets away from the electrode. We obtained similar results in BLG, as shown in Fig. 4(b) and (d). The appearance of the D peak is definitely due to the Au thin film deposition process on graphene as the deposition of Ti does not introduce many defects to the graphene lattice. The appearance of the Raman D peak of graphene after directly depositing gold onto graphene has been reported in previous results.[40,41] During the deposition, Au atoms may have higher kinetic energy than Ti atoms. In order to analyze the D peak induced by Au deposition, we adapted the integrated intensity ratio of D and G bands (I_D/I_G), which probes the intervalley scattering rate of distributed disorder. We can

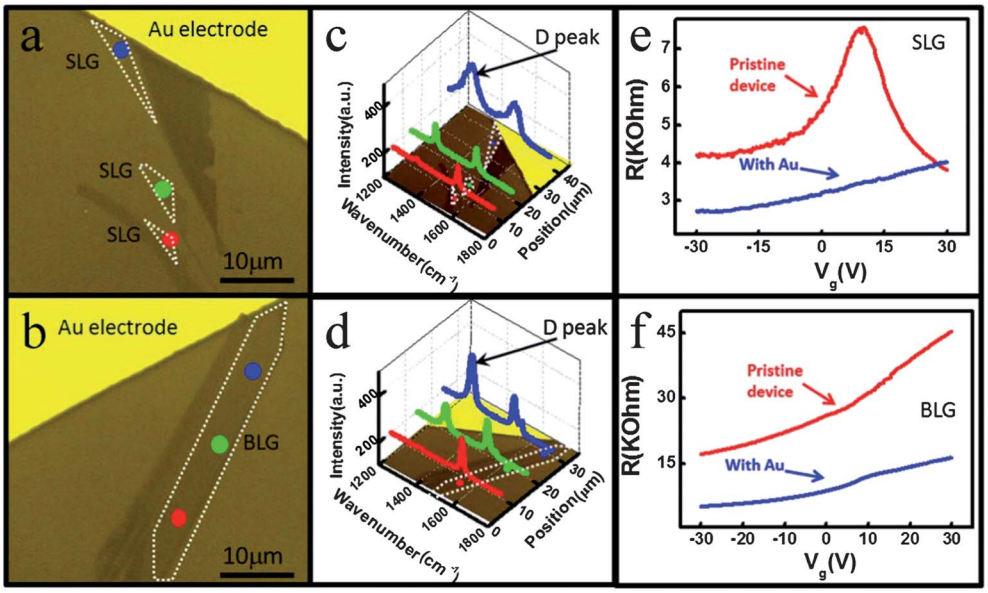

Fig. 4 Direct deposition of Au would induce defects to SLG and BLG. (a) Optical image of a graphene sample with Ti/Au contact electrode. (c) Raman spectra of three positions of the SLG samples in (a). (b) Optical image of the bilayer graphene sample with Ti/Au contact electrodes. (d) Raman spectra of three positions of the BLG samples in (b). The SLG and BLG regions are illustrated by the dashed line frames. (e) Relationships of resistance and back gate voltage of SLG device before and after Au deposition. (f) Relationships of resistance and back gate voltage of BLG device before and after Au deposition.

estimate the average distance between the scatters by using the empirical relationship established for the determination of the crystallite size L_α of nanographene by Raman spectroscopy[19,42]

$$L_\alpha = (2.4 \times 10^{-10})\lambda_L{}^4 \left(I_D / I_G\right)^{-1} \quad (1)$$

where $\lambda_L = 532$ nm represents the wavelength of the excitation laser. The formula yields $L_\alpha = 22.3$ nm for $I_D/I_G = 0.867$ (green spot in Fig. 4(a)) and the value of L_α provides information about the average scattering distance in the disordered graphene. Although Raman spectroscopy at $\lambda_L = 532$ nm probes the scattering rates at the energy one order of magnitude larger than the typical Fermi level in transport experiments, one can expect that L_α is equal to the transport mean free path l for carriers in the large-angle scattering.[43] In this way, one could efficiently estimate the carrier mobility through Raman peaks. For Dirac fermions, one can write carrier mobility[43]

$$\mu = \frac{le v_F}{E_F} = (2.4 \times 10^{-10}) \frac{e v_F}{E_F} \lambda_L{}^4 \left(I_D / I_G\right)^{-1} \quad (2)$$

where $v_F \approx 10^6$ ms^{-1} is the Fermi velocity and $e \approx 1.6 \times 10^{-19}$ C is the elementary charge. Assuming the electrons and holes were generated at $\lambda_L = 532$ nm, their energies locate at $E_F = 1.17$ eV with $l \approx L_\alpha = 22.3$ nm. The carrier mobility can be achieved: $\mu \approx 191$ cm^2 V^{-1} s^{-1}. This result indicates that the deposition of Au atoms can greatly degrade the quality of graphene. Electrical measurements were carried out to analyze the influence of Au deposition. Fig. 4(e) shows the relationship of the resistance *versus* back gate voltage in a pristine SLG device before and after Au deposition. The NP of the pristine SLG device is 10 V while the device with Au coating has a NP larger than 30 V. It indicates that Au could induce p-type doping in monolayer graphene, the charge transfer between Au and graphene is caused by their work function difference[36–38] ($\varphi_{graphene} \sim 4.5$ eV and $\varphi_{Au} \sim 5.1$ eV). Mobility of the SLG device has been extracted by the following formula:[44]

$$R_{Total} = R_{contact} + \frac{L}{We\mu\sqrt{n_0{}^2 + n^2}}, n = \frac{C|V_g - V_{Dirac}|}{e} \quad (3)$$

where R_{Total} is the total resistance. L and W represent the length and width of the device, respectively. n means the carrier density and n_0 is the residual carrier concentration in the device. μ is the mobility of the device. $C = 1.15 \times 10^{-4}$ F m^{-1} is the capacitance of 300 nm SiO_2. The extracted carrier (hole) mobility of the pristine SLG device is about 4200 cm^2 V^{-1} s^{-1} while carrier (hole) mobility of the device after Au deposition decreases to 568 cm^2 V^{-1} s^{-1}. From Raman spectra, an obvious Raman D peak was observed in the SLG device with Au coating. We estimated the carrier mobility by using the integrated intensity ratio of D and G bands of this SLG device,[43] $I_D/I_G = 0.282$ corresponds to $\mu \approx 582$ cm^2 V^{-1} s^{-1}. The carrier mobility derived from Raman results matches well with the one obtained from electrical measurement for the same sample. Fig. 4(f) shows the R–V_g relationship for BLG device. By fitting the curves, the hole mobilities of the BLG device before and after the Au deposition are 2426 cm^2 V^{-1} s^{-1} and 616 cm^2 V^{-1} s^{-1}, respectively. In summary, it is necessary to optimize the evaporation process to reduce the damage of metal atoms to the graphene lattice.

To conclude, we have investigated the effects of electron beam irradiation and metal deposition on the graphene lattice in actual nanofabrication processing. Both of them could induce disorder to the graphene lattice. Severe electron beam irradiation could introduce amorphous carbon deposition,

which is usually ignored in previous studies. In real EBL processing, the electron beam with high energy may directly damage the lattice structure of graphene by knocking off carbons or activating the reaction between graphene and substrate. Bilayer graphene exhibits higher stability under e-beam irradiation than monolayer graphene does. In the formation of metallic contacts, Ti could not induce defects in graphene while Au remarkably damaged the graphene lattice. These experimental results reveal the influence of fabrication processing on the graphene lattice and may be beneficial for the optimization of processes.

Acknowledgements

This work is supported by the Singapore National Research Foundation under NRF RF award no. NRF-RF2010-07 and MOE Tier 2 MOE2009-T2-1-037.

References

1 Y. H. Wu, T. Yu and Z. X. Shen, *J. Appl. Phys.*, 2010, **108**, 071301.
2 I. Childres, L. A. Jauregui, M. Foxe, J. F. Tian, R. Jalilian, I. Jovanovic and Y. P. Chen, *Appl. Phys. Lett.*, 2010, **97**, 173109.
3 D. Teweldebrhan and A. A. Balandin, *Appl. Phys. Lett.*, 2009, **94**, 013101.
4 D. Teweldebrhan and A. A. Balandin, *Appl. Phys. Lett.*, 2009, **95**, 246102.
5 Y. H. He, L. Wang, X. L. Chen, Z. F. Wu, W. Li, Y. Cai and N. Wang, *Appl. Phys. Lett.*, 2011, **99**, 033109.
6 K. J. Kim, J. H. Choi, H. Lee, H. K. Lee, T. H. Kang, Y. H. Han, B. C. Lee, S. Kim and B. Kim, *J. Phys. Chem. C*, 2008, **112**, 13062–13064.
7 M. S. Xu, D. Fujita and N. Hanagata, *Nanotechnology*, 2010, **21**, 265705.
8 J. D. Jones, K. K. Mahajan, W. H. Williams, P. A. Ecton, Y. Mo and J. M. Perez, *Carbon*, 2010, **48**, 2335–2340.
9 J. H. Chen, W. G. Cullen, C. Jang, M. S. Fuhrer and E. D. Williams, *Phys. Rev. Lett.*, 2009, **102**, 236805.
10 K. M. McCreary, K. Pi, A. G. Swartz, W. Han, W. Bao, C. N. Lau, F. Guinea, M. I. Katsnelson and R. K. Kawakami, *Phys. Rev. B: Condens. Matter Mater. Phys.*, 2010, **81**, 115453.
11 K. Pi, K. M. McCreary, W. Bao, W. Han, Y. F. Chiang, Y. Li, S. W. Tsai, C. N. Lau and R. K. Kawakami, *Phys. Rev. B: Condens. Matter Mater. Phys.*, 2009, **80**, 075406.
12 Z. H. Ni, H. M. Wang, T. Yu and Z. X. Shen, *Nano Lett.*, 2007, **7**, 2758–2763.
13 A. C. Ferrari, J. C. Meyer, V. Scardaci, C. Casiraghi, M. Lazzeri, F. Mauri, S. Piscanec, D. Jiang, K. S. Novoselov, S. Roth and A. K. Geim, *Phys. Rev. Lett.*, 2006, **97**, 187401.
14 J. C. Meyer, C. Kisielowski, R. Erni, M. D. Rossell, M. F. Crommie and A. Zettl, *Nano Lett.*, 2008, **8**, 3582–3586.
15 A. Hashimoto, K. Suenaga, A. Gloter, K. Urita and S. Iijima, *Nature*, 2004, **430**, 870–873.
16 L. Li, S. Reich and J. Robertson, *Phys. Rev. B: Condens. Matter Mater. Phys.*, 2005, **72**, 184109.
17 J. D. Jones, P. A. Ecton, Y. Mo and J. M. Perez, *Appl. Phys. Lett.*, 2009, **95**, 246101.
18 G. X. Liu, D. Teweldebrhan and A. A. Balandin, *IEEE Trans. Nanotechnol.*, 2011, **10**, 865–870.
19 A. C. Ferrari and J. Robertson, *Phys. Rev. B: Condens. Matter Mater. Phys.*, 2000, **61**, 14095–14107.
20 J. C. Meyer, C. O. Girit, M. F. Crommie and A. Zettl, *Appl. Phys. Lett.*, 2008, **92**, 123110.
21 H. W. Conru and P. C. Laberge, *J. Phys. E: Sci. Instrum.*, 1975, **8**, 136–138.
22 D. C. Elias, R. R. Nair, T. M. G. Mohiuddin, S. V. Morozov, P. Blake, M. P. Halsall, A. C. Ferrari, D. W. Boukhvalov, M. I. Katsnelson, A. K. Geim and K. S. Novoselov, *Science*, 2009, **323**, 610–613.
23 Z. Q. Luo, T. Yu, Z. H. Ni, S. H. Lim, H. L. Hu, J. Z. Shang, L. Liu, Z. X. Shen and J. Y. Lin, *J. Phys. Chem. C*, 2011, **115**, 1422–1427.
24 A. M. Lanzillotto, T. E. Madey and R. A. Baragiola, *Phys. Rev. Lett.*, 1991, **67**, 232–235.
25 O. Lehtinen, J. Kotakoski, A. V. Krasheninnikov, A. Tolvanen, K. Nordlund and J. Keinonen, *Phys. Rev. B: Condens. Matter Mater. Phys.*, 2010, **81**, 153401.
26 J. Y. Fan, J. M. Michalik, L. Casado, S. Roddaro, M. R. Ibarra and J. M. De Teresa, *Solid State Commun.*, 2011, **151**, 1574–1578.
27 R. J. Hawryluk, A. M. Hawryluk and H. I. Smith, *J. Appl. Phys.*, 1974, **45**, 2551–2566.
28 R. J. Hawryluk, H. I. Smith, A. Soares and A. M. Hawryluk, *J. Appl. Phys.*, 1975, **46**, 2528–2537.
29 A. Das, S. Pisana, B. Chakraborty, S. Piscanec, S. K. Saha, U. V. Waghmare, K. S. Novoselov, H. R. Krishnamurthy, A. K. Geim, A. C. Ferrari and A. K. Sood, *Nat. Nanotechnol.*, 2008, **3**, 210–215.
30 K. Reichelt and X. Jiang, *Thin Solid Films*, 1990, **191**, 91–126.
31 T. Asano, N. Uetake and K. Suzuki, *J. Nucl. Sci. Technol.*, 1992, **29**, 1194–1200.
32 G. Giovannetti, P. A. Khomyakov, G. Brocks, V. M. Karpan, J. van den Brink and P. J. Kelly, *Phys. Rev. Lett.*, 2008, **101**, 026803.
33 N. Peimyoo, T. Yu, J. Z. Shang, C. X. Cong and H. P. Yang, *Carbon*, 2012, **50**, 201–208.
34 P. A. Khomyakov, G. Giovannetti, P. C. Rusu, G. Brocks, J. van den Brink and P. J. Kelly, *Phys. Rev. B: Condens. Matter Mater. Phys.*, 2009, **79**, 195425.
35 N. Peimyoo, J. W. Li, J. Z. Shang, X. N. Shen, C. Y. Qiu, L. H. Xie, W. Huang and T. Yu, *ACS Nano*, 2012, **6**, 8878–8886.
36 N. Ooi, A. Rairkar and J. B. Adams, *Carbon*, 2006, **44**, 231–242.
37 S. J. Sque, R. Jones and P. R. Briddon, *Phys. Status Solidi A*, 2007, **204**, 3078–3084.
38 H. B. Michaelson, *J. Appl. Phys.*, 1977, **48**, 4729–4733.
39 C. X. Cong, T. Yu, Z. H. Ni, L. Liu, Z. X. Shen and W. Huang, *J. Phys. Chem. C*, 2009, **113**, 6529–6532.

40 Y. Y. Wang, Z. H. Ni, H. L. Hu, Y. F. Hao, C. P. Wong, T. Yu, J. T. L. Thong and Z. X. Shen, *Appl. Phys. Lett.*, 2010, **97**, 163111.
41 H. Q. Zhou, C. Y. Qiu, Z. Liu, H. C. Yang, L. J. Hu, J. Liu, H. F. Yang, C. Z. Gu and L. F. Sun, *J. Am. Chem. Soc.*, 2010, **132**, 944–946.
42 L. G. Cancado, K. Takai, T. Enoki, M. Endo, Y. A. Kim, H. Mizusaki, A. Jorio, L. N. Coelho, R. Magalhaes-Paniago and M. A. Pimenta, *Appl. Phys. Lett.*, 2006, **88**, 163106.
43 Z. H. Ni, L. A. Ponomarenko, R. R. Nair, R. Yang, S. Anissimova, I. V. Grigorieva, F. Schedin, P. Blake, Z. X. Shen, E. H. Hill, K. S. Novoselov and A. K. Geim, *Nano Lett.*, 2010, **10**, 3868–3872.
44 B. C. Huang, M. Zhang, Y. J. Wang and J. Woo, *Appl. Phys. Lett.*, 2011, **99**, 032107.

